

# Analyst

Accepted Manuscript



This is an *Accepted Manuscript*, which has been through the Royal Society of Chemistry peer review process and has been accepted for publication.

*Accepted Manuscripts* are published online shortly after acceptance, before technical editing, formatting and proof reading. Using this free service, authors can make their results available to the community, in citable form, before we publish the edited article. We will replace this *Accepted Manuscript* with the edited and formatted *Advance Article* as soon as it is available.

You can find more information about *Accepted Manuscripts* in the [Information for Authors](#).

Please note that technical editing may introduce minor changes to the text and/or graphics, which may alter content. The journal's standard [Terms & Conditions](#) and the [Ethical guidelines](#) still apply. In no event shall the Royal Society of Chemistry be held responsible for any errors or omissions in this *Accepted Manuscript* or any consequences arising from the use of any information it contains.

## Nanopipette Delivery: Influence of Surface Charge

Cite this: DOI: 10.1039/x0xx00000x

Wenqing Shi, Niya Sa, Rahul Thakar, Lane A. Baker\*

Received 00th January 2012,  
Accepted 00th January 2012

DOI: 10.1039/x0xx00000x

www.rsc.org/

In this report, transport through a nanopipette is studied and the interplay between current rectification and ion delivery for small pipettes is examined. First, surface charge dependence of concentration polarization effects in a quartz nanopipette was investigated. Electrical characterization was performed through current-potential (I-V) measurements. In addition, fluorescein (an anionic fluorescent probe) was utilized to optically map ion enrichment and ion depletion in the nanopipette tip. Bare nanopipettes and polyethylenimine (PEI)-modified nanopipettes were examined. Results confirm that concentration polarization is a surface charge dependent phenomenon and delivery can be controlled through modification of surface charge. The relationship between concentration polarization effects and voltage-driven delivery of charged electroactive species was investigated with a carbon ring/nanopore electrode fabricated from pyrolyzed parylene C (PPC). Factors such as surface charge polarity of the nanopipette, electrolyte pH, and electrolyte concentration were investigated. Results indicate that with modification of surface charge, additional control over delivery of charged species can be achieved.

### Introduction

Pipettes with tip openings on the scale of tens to hundreds of nanometers, hereafter referred to as nanopipettes, have been utilized in a wide variety of fundamental and applied studies related to nanoscale ion transport.<sup>1-8</sup> In particular, the ability of nanopipettes to manipulate ultrasmall volumes and to act as a molecular reservoir to deposit and deliver biomolecules is of great interest. Controllable voltage-driven delivery of biomolecules via nanopipette has been demonstrated in a number of experiments,<sup>3,7,9-17</sup> which include highly-localized deposition of DNA or proteins,<sup>9,10</sup> targeted nano-injection,<sup>11</sup> voltage-controlled attoliter fluid manipulation,<sup>18</sup> drug delivery<sup>12</sup> and surface patterning.<sup>9,10,15,16</sup> Despite advantages of nanopipettes as delivery tools (e.g. small size, low-cost fabrication), efforts to improve quantitative aspects of delivery and expand pipette functionality are desirable.

To develop a quantitative nanoscale delivery tool, the amount of molecules delivered by the nanopipette must be determined. Previously, Korchev, Klenerman and coworkers have demonstrated the ability of nanopipettes for programmable delivery of biomolecules (e.g., DNA, proteins), in which additional fluorescent markers enabled the determination of amount of biomolecules ejected.<sup>7,9,10,15,19</sup> Recently, Korchev and coworkers investigated the influence of nanopipette size, applied voltage and probe-substrate distance on quantitative nanopipette delivery.<sup>3</sup> In addition, with larger (micro) pipettes, carbon fiber electrodes coupled to multiple delivery barrels have been used for simultaneous detection of the iontophoretic delivery of drug molecules.<sup>20-22</sup> Addition of a carbon fiber electrode near the

delivery barrel allows measurement of the local concentration of electroactive molecules delivered.<sup>20-24</sup> The number of molecules delivered depends on factors such as the applied delivery potential and the size of the pipette tip opening.<sup>3</sup> The surface charge of the nanopipette is also an important factor that has received little attention. At larger scales, the surface charge of the pipette wall does not impose a significant effect on the concentration of ions in the delivery channel.<sup>20-24</sup> As demonstrated in previous reports, when channel dimensions shrink to small scales, surface-charge controlled concentration polarization becomes a dominant factor in ion transport.<sup>2,6,25-32</sup>

Here, we demonstrate a carbon ring/nanopore electrode geometry and unambiguously demonstrate the importance of surface charge and analyte charge for nanopipettes used for voltage-driven delivery. To quantify delivery of electroactive species, a carbon ring/nanopore electrode was fabricated at the tip of the nanopipette. Typical electrode configurations consisted of a carbon ring (200-300 nm thickness, pyrolyzed carbon) which surrounds an open pore (200 nm radius) at the tip of a quartz nanopipette.<sup>33-36</sup> An example of an electrode utilized in these studies is shown in **Figure 1a**. Detection of localized voltage-driven delivery experiments with charged electroactive species were performed, where the central pore of the nanopipette was used for delivery and the surrounding carbon ring recorded the delivery process. Results suggest that surface charge of the nanopipette plays a significant role, with enhanced or diminished delivery of charged species controlled by pipette surface charge. These findings underscore the importance of surface charge for future work that makes use of nanopipette delivery tools.

## Experimental

Chemicals, materials, and detailed procedures for nanopipette fabrication, current-voltage (I-V) measurements, fluorescence microscopy imaging and polyethylenimine (PEI) surface modification<sup>37</sup> are detailed in sections SI-1 to SI-5 of the Supporting Information.

### Fabrication of carbon ring/nanopore electrode

Nanopipettes were prepared as described in SI-2 (Supporting Information). Parylene C was used as the deposition material and a four-step procedure was used to fabricate the carbon ring/nanopore electrode, as described previously.<sup>33-36</sup> Nanopipettes were placed in the deposition chamber of a parylene deposition system (PDS 2010, SCS coating, Indianapolis, IN) in an upright position and chemical vapor deposition of parylene C (PC) on the nanopipette surface was carried out with vaporizer and furnace temperature settings at 175°C and 690°C, respectively. PC-coated nanopipettes were then pyrolyzed at 900°C under inert N<sub>2</sub> flow for 1 h to obtain pyrolyzed parylene C (PPC). PPC-coated nanopipettes were then immersed in A-174 silane adhesion promotion solution (Supporting Information SI-6) for 15 min, followed by a thorough wash with isopropyl alcohol. Next, a second layer of PC was applied to the PPC-coated pipettes for complete insulation. Finally, a Zeiss Auriga® Modular Cross Beam work station (Oberkochen, Germany) was used to mill the insulated electrodes. The "Mill for Depth" function was selected in SmartSEM® V05.05 XB operating software. A 100 µm depth and a 30 kV, 600 pA beam current was used. A detailed description of electrode characterization can be found in SI-7 (Supporting information).

### Voltage-driven delivery by nanopipettes

The voltage-driven delivery experimental setup is depicted in Figure 1b. Carbon ring/nanopore electrodes were backfilled with equal concentrations (2 mM) of both (ferrocenylmethyl) trimethylammonium (FcTMA<sup>+</sup>) and ferricyanide (Fe(CN)<sub>6</sub><sup>3-</sup>) together with KCl as the supporting electrolyte (electrolytes used were 100 mM, pH 8.0; 500 mM, pH 8.0 and 100 mM, pH 5.5 as specified in the Results and Discussion.) In addition, in separate experiments, the pipette was filled with a neutral electroactive species, ferrocen methanol (FcMeOH), together with 100 mM KCl (pH = 8.0). The bath solution contained supporting electrolyte. A square-wave potential was generated by a function generator (33220A Agilent, Santa Clara, CA) and applied to the Ag/AgCl electrode inside the nanopipette, termed as the delivery electrode (DE), with respect to the instrument ground. Analyte molecules were then iontophoretically delivered out of the pipette aperture by selection of the applied potential. For instance, cationic FcTMA<sup>+</sup> was delivered from the pipette by positive applied potentials while anionic Fe(CN)<sub>6</sub><sup>3-</sup> was delivered by application of negative potentials to the DE.

### Simultaneous electrochemical detection by the carbon ring electrode

A model CH910B potentiostat (CH Instruments, Austin, TX)

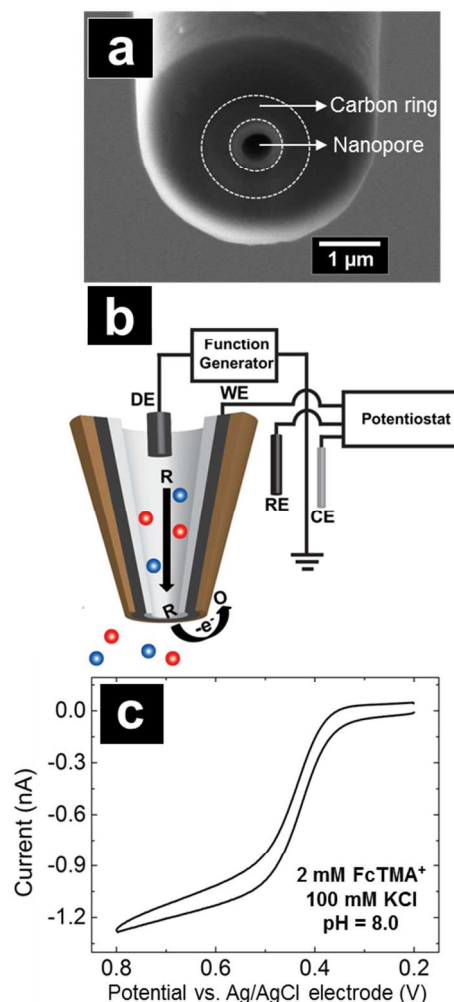


**Figure 1.** (a) SEM image of an end-on view of the carbon ring/nanopore electrode, dashed white line indicates inner and outer ring of carbon electrode, added for clarity; (b) Instrument set-up; (c) Cyclic voltammogram (CV) of 2 mM FcTMA<sup>+</sup> with 100 mM KCl, pH = 8.0, scan rate = 0.1 V/s.

housed inside a grounded faraday cage was used. Amperometry and voltammetry were performed with a three-electrode system (Figure 1b). A Ag/AgCl reference electrode (RE) and a Pt wire counter electrode (CE) were used. The carbon ring electrode around the pipette aperture served as the working electrode (WE) for quantitation of delivery. The WE potential was at a sufficiently positive/negative value to oxidize or reduce electroactive species of interest at the WE directly after delivery. The relative amount of molecules delivered could then be determined by monitoring the current amplitude at the WE. For experiments here, delivery for cations/anions was compared within a single electrode, and as such the relative quantity of species delivered was compared, as opposed to the absolute amount. A cyclic voltammogram, shown in Figure 1c, was taken in 2 mM FcTMA<sup>+</sup> with 100 mM KCl (pH = 8.0) by the carbon ring electrode (WE) with respect to a Ag/AgCl electrode, and a steady-state current was

Analyst

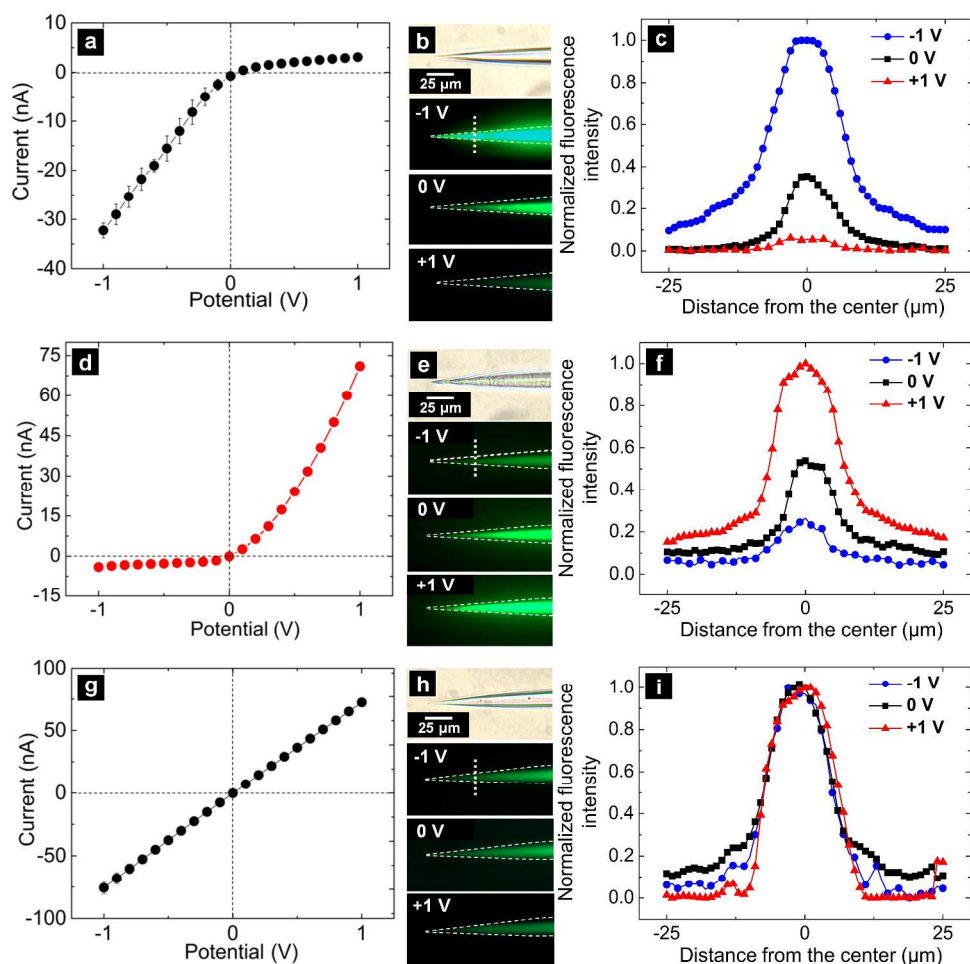


**Figure 2.** (a) I-V response for a bare pipette filled with 50 mM KCl and 200  $\mu\text{M}$  fluorescein, pH = 8.0; (b) Bright-field image of pipette tip, fluorescence microscopy images of the pipette tip at -1 V, 0 V and +1 V; (c) Fluorescence intensity profile along the white dashed line drawn in 2b (-1 V); (d) I-V response for PEI-modified pipette filled with 50 mM KCl and 200  $\mu\text{M}$  fluorescein, pH = 8.0; (e) Bright-field image of the pipette tip; fluorescence microscopy images of the pipette tip at -1 V, 0 V and +1 V; (f) Fluorescence intensity profile along the white dashed line drawn in 2e (-1 V); (g) I-V response for bare pipette filled with 500 mM KCl and 200  $\mu\text{M}$  fluorescein, pH = 8.0; (h) Bright-field image of the pipette tip, fluorescence microscopy images of pipette tip at -1 V, 0 V and +1 V; (i) Fluorescence intensity profile along the white dashed line drawn in 2h (-1 V).

obtained at 0.8 V. Therefore, during the delivery/detection cycle for  $\text{FcTMA}^+$ , the WE potential was set at 0.8 V such that the delivered  $\text{FcTMA}^+$  was oxidized to  $\text{FcTMA}^{2+}$  instantly. The predicted faradic current value for a planar carbon ring electrode with dimensions the same as the electrode prepared in this experiment is obtained from **equation 1**,<sup>38</sup> in which  $n$  is the number of electrons transferred;  $F$  is the Faraday constant;  $D$  is the diffusion coefficient ( $6.0 \times 10^{-6} \text{ cm}^2 \cdot \text{s}^{-1}$  for  $\text{FcTMA}^+$ )<sup>39</sup> and  $C$  is the concentration of electroactive species. Variables  $a$  and  $b$  are the inner and the outer radius of the carbon ring electrode, respectively.

$$I_{ss} = nFDC \left[ \frac{\pi^2(a+b)}{\ln\left[32\left(\frac{a}{b-a}\right)\right] + \exp\left(\frac{\pi^2}{4}\right)} \right] \quad (1)$$

The calculated response of the carbon electrode ( $a = 390 \text{ nm}$ ,  $b = 820 \text{ nm}$ ) was 0.937 nA compared to an experimentally measured current value of 1.243 nA. The discrepancy suggests there are subtle differences arise for electrodes prepared here due to the presence of the central nanopore, in the actual and measured electrode dimensions or from incomplete sealing at the interface of the parylene/pyrolyzed parylene layers, and possibly the relatively thin width of the parylene layer. Either of these situations should not influence the results reported here.

## Results and Discussion

### Surface charge dependent accumulation and depletion of charge carriers

Ion current rectification (ICR) effects are induced by ion concentration polarization in the confined geometry of a nanopipette. The resultant conductance difference at potentials of different polarity can be observed as asymmetry in the current-voltage response, as measured through I-V curves.<sup>40-42</sup> To further visualize surface charge dependent concentration polarization in the pipette tip, nanopipettes were filled with a solution of an anionic fluorescent probe (fluorescein) to optically map ion enrichment and ion depletion in the tip region.<sup>28, 29</sup> These effects were studied for nanopipettes under a range of conditions (e.g., surface charge polarity, electrolyte concentration), as shown in **Figure 2 (a-i)**. For bare nanopipettes filled with 50 mM KCl (pH = 8.0) and 200  $\mu\text{M}$  fluorescein, ion current was rectified such that larger current was measured at negative applied potentials (**Figure 2a**). Concentration polarization at different applied potentials was observed, as verified in **Figure 2b**. When -1 V was applied to the pipette electrode, fluorescein accumulation in the tip region is evident, and when +1 V was applied, depletion is observed. Experimental results obtained here are in good agreement with previous reports for quartz nanopipettes and nanochannels with negative surface charge.<sup>2, 6, 28, 29, 31, 32</sup>

Surface charge at a nanoscale tip plays an important role in controlling ion selectivity of the tip, which further controls the concentration polarization effect and eventually determines tip conductivity. The dependence of the concentration polarization effect on surface charge was investigated by altering the pipette surface charge from negative to positive with PEI modification.<sup>37</sup> For PEI-modified pipettes filled with 50 mM KCl and 200  $\mu$ M fluorescein, reversed ion current rectification was obtained (**Figure 2d**), where ion current was shown to be larger at positive applied potentials with respect to the corresponding negative applied potentials. Reversed concentration polarization was also observed (**Figure 2e**) optically. Ion accumulation occurred inside the pipette at +1 V, while ion depletion took place at -1 V, which was in good agreement with the conductance response observed in the I-V curve (**Figure 2d**).

A control experiment was performed at higher electrolyte concentration (500 mM KCl, pH = 8.0, with 200  $\mu$ M fluorescein), where surface charge effects were screened. In **Figure 2g**, a linear I-V response was recorded for a nanopipette filled with 500 mM KCl. From **Figure 2h**, the fluorescence intensity stayed nearly identical at applied potentials of -1 V, 0 V and +1 V, which indicates no observable concentration polarization occurred. These results further indicate that selectivity in ion transport through the pipette orifice is removed once surface charge at the nanopipette is screened.

Normalized fluorescence intensity distribution was plotted along the dashed line drawn across the pipette tip region, as shown in **Figures 2b** (-1 V), **2e** (-1 V) and **2h** (-1 V). For bare nanopipettes, at 50 mM KCl, the fluorescence intensity at -1 V (blue trace) is higher compared to that at 0 V potential (black trace), while the lowest fluorescence intensity was observed under +1 V (red trace) (**Figure 2c**). PEI-modified nanopipettes filled with 50 mM electrolyte displayed a reversed concentration polarization effect, where the highest fluorescence intensity was observed at positive potentials, and the lowest fluorescence intensity was observed at negative potentials (**Figure 2f**). At 500 mM electrolyte concentration, the normalized fluorescence intensity remained relatively constant at different applied potentials (**Figure 2i**).

Results described above can be explained on the basis of the prevailing model of ion current rectification in nanodevices.<sup>2, 5, 29, 31, 37, 41, 42</sup> For bare quartz surfaces at moderate to high pH,<sup>43</sup> deprotonated silanol groups result in a negative surface charge. Presence of negative surface charge leads to preferential enhancement/depletion of charged species. This effect can be reversed with a positively charged surface, represented here as PEI-modified pipettes. In the context of experiments here, for bare nanopipettes with negative surface charge, ions accumulate in the nanopipette tip under negative applied potentials and deplete at positive applied potentials.

For PEI-modified nanopipettes with positive surface charge, ion accumulation takes place at positive applied potentials while ion depletion is observed at negative applied potentials.

#### Dependence of voltage-driven delivery on the concentration polarization effect

To further understand concentration polarization effects on voltage-driven delivery from nanopipettes and to examine whether the delivery of charged species can be manipulated through control of pipette surface charge, negatively charged  $\text{Fe}(\text{CN})_6^{3-}$  and positively charged  $\text{FcTMA}^+$  were utilized as anionic and cationic redox probes. These probes were chosen as they fill the prerequisites of non-overlapping redox potentials and comparable diffusion coefficients ( $6.0 \times 10^{-6} \text{ cm}^2 \cdot \text{s}^{-1}$  for  $\text{FcTMA}^+$  and  $7.6 \times 10^{-6} \text{ cm}^2 \cdot \text{s}^{-1}$  for  $\text{Fe}(\text{CN})_6^{3-}$ ).<sup>39, 44</sup>

Solutions of equal concentration (2 mM) of  $\text{FcTMA}^+$  and  $\text{Fe}(\text{CN})_6^{3-}$  together with KCl supporting electrolyte were used to fill the nanopipettes. To accomplish voltage-driven delivery, a square wave with peak value  $V_p = \pm 0.5 \text{ V}$  and frequency of 0.1 Hz was applied to the delivery electrode to iontophoretically dispense the charged electroactive molecules out of the nanopipette reservoir. To quantify the amount of molecules delivered, the carbon ring electrode (WE) was set to a potential at which the redox reaction of interest occurs. During the delivery/detection cycle for cationic  $\text{FcTMA}^+$ , +0.5 V was the delivery potential while -0.5 V was the retaining potential applied to DE. WE was biased at 0.8 V for oxidation of delivered  $\text{FcTMA}^+$ . In the delivery/detection cycle for anionic  $\text{Fe}(\text{CN})_6^{3-}$ , -0.5 V was the delivery potential and +0.5 V was the retaining potential applied to DE, the WE was biased at -0.8 V such that  $\text{Fe}(\text{CN})_6^{3-}$  delivered could be reduced to  $\text{Fe}(\text{CN})_6^{4-}$ . Faradaic current was measured simultaneously at the WE while a square wave potential was applied to the DE. Amperometric current-time (I-T) responses for both  $\text{FcTMA}^+$  and  $\text{Fe}(\text{CN})_6^{3-}$  at WE were recorded and plotted (**Figures 3b, 3d, 3f**).

In **Figure 3a**, a bare nanopipette was filled with 100 mM KCl supporting electrolyte, buffered at pH 8.0 and displayed a rectified current response. I-T curves for both species are shown in **Figure 3b**. A significantly larger (7.5-fold) faradaic current for anionic  $\text{Fe}(\text{CN})_6^{3-}$  ( $|I_{\text{Fe}(\text{CN})_6^{3-}}| = 150 \text{ pA}$ ) was observed compared to the current for cationic  $\text{FcTMA}^+$  ( $|I_{\text{FcTMA}^+}| = 20 \text{ pA}$ ), which indicates that a larger quantity of  $\text{Fe}(\text{CN})_6^{3-}$  was delivered compared to  $\text{FcTMA}^+$ . To explain the enhanced delivery for  $\text{Fe}(\text{CN})_6^{3-}$  and diminished delivery for  $\text{FcTMA}^+$ , for pipettes with negative surface charge, both cations and anions accumulate at negative potentials and deplete at positive potentials. Anionic species ( $\text{Fe}(\text{CN})_6^{3-}$ ) will accumulate in the tip prior to ejection under negative potentials (during application of a retaining potential), whereas cationic species ( $\text{FcTMA}^+$ ) are depleted in the tip region prior to ejection when a positive potential is applied.

PEI-modified carbon ring/nanopore electrodes were examined also. In **Figure 3c**, the I-V response for PEI-modified nanopipettes filled with 100 mM KCl exhibited a reversed rectified response, the same as the previous observation in the surface charge dependent concentration polarization study (**Figure 2d**). From I-T curves in **Figure 3d**,  $|I_{FcTMA^+}|$  (110 pA) is 11 times larger than  $|I_{Fe(CN)_6^{3-}}|$  (10 pA). This is as expected, since for a PEI-modified pipette, ion accumulation occurs at positive potentials, which leads to an increased amount of  $FcTMA^+$  in the tip region and therefore enhanced delivery for  $FcTMA^+$ . Ion depletion takes place at negative potentials which results in a reduced amount of  $Fe(CN)_6^{3-}$  in the tip region, and further leads to the diminished delivery of  $Fe(CN)_6^{3-}$ .

Concentration polarization in the confined geometry is assumed to be the cause for the charge-dependent delivery of charged redox probes in both bare and PEI-modified nanopipettes. To further prove the hypothesis, an additional control experiment was performed with 100 mM KCl supporting electrolyte buffered at pH = 5.5, where the majority of the silanol groups on the quartz nanopipette surface were protonated and the pipette surface was considered to be neutral. As a result, the current rectification effect diminished (**Figure S2(a), Supporting Information**). In the I-T curves (**Figure S2(b), Supporting Information**), the current magnitudes for  $FcTMA^+$  and  $Fe(CN)_6^{3-}$  were comparable,  $|I_{Fe(CN)_6^{3-}}| = 310 \text{ pA}$  and  $|I_{FcTMA^+}| = 290 \text{ pA}$ .

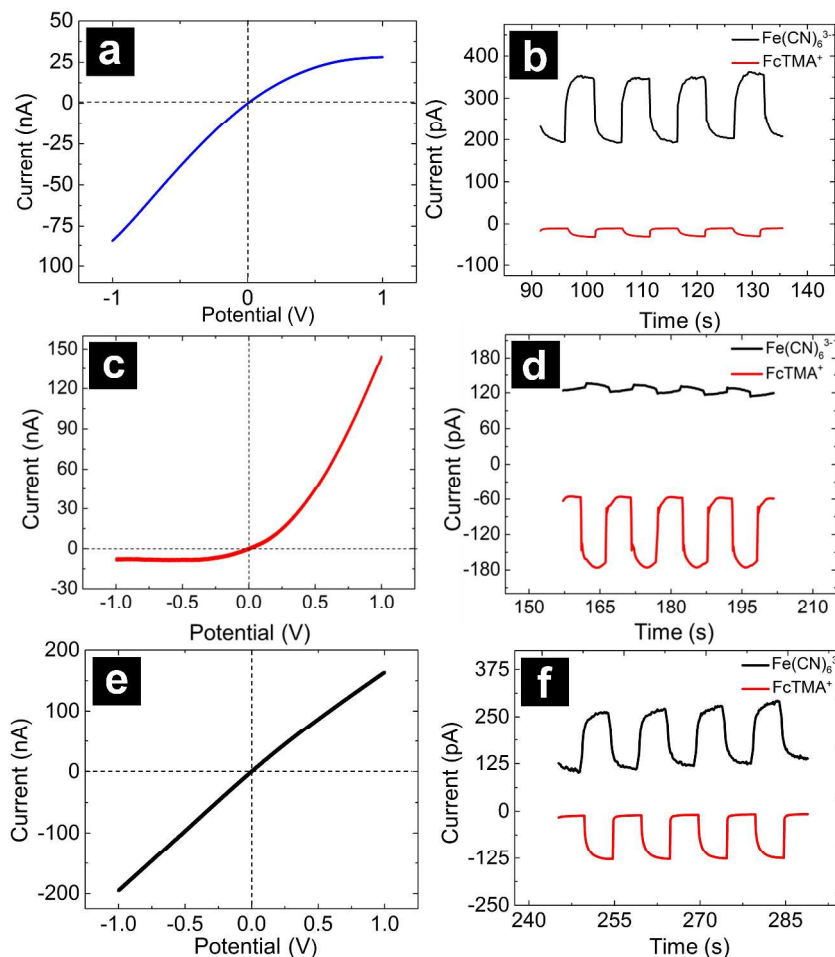


**Figure 3.** (a) I-V response of the carbon ring/nanopore electrode filled with 100 mM KCl together with 2 mM  $Fe(CN)_6^{3-}$  and  $FcTMA^+$ , pH = 8.0; (b) Amperometric current-time (I-T) traces collected by the carbon ring electrode for  $Fe(CN)_6^{3-}$  and  $FcTMA^+$ , pH = 8.0; (c) I-V response of the PEI-modified carbon ring/nanopore electrode filled with 100 mM KCl together with 2 mM  $Fe(CN)_6^{3-}$  and  $FcTMA^+$ , pH = 8.0; (d) I-T traces collected by the carbon ring electrode for  $Fe(CN)_6^{3-}$  and  $FcTMA^+$ . (e) I-V response of the carbon ring/nanopore electrode filled with 500 mM KCl together with 2 mM  $Fe(CN)_6^{3-}$  and  $FcTMA^+$ , pH = 8.0; (f) I-T traces collected by the carbon ring electrode for  $Fe(CN)_6^{3-}$  and  $FcTMA^+$ . (note: data shown is from representative pipettes, not a single pipette.)

As a control experiment, to represent the situation where the influence of surface charge is negligible, or the surface charge effect is screened, a bare nanopipette filled with 500 mM KCl was tested. In **Figure 3e**, the I-V response is shown to be linear. In the I-T curves (**Figure 3f**), the current magnitudes for  $FcTMA^+$  and  $Fe(CN)_6^{3-}$  are comparable,  $|I_{Fe(CN)_6^{3-}}| = 130 \text{ pA}$  and  $|I_{FcTMA^+}| = 120 \text{ pA}$ , which indicates the amount of delivered cationic  $FcTMA^+$  and anionic  $Fe(CN)_6^{3-}$  is nearly the same.

These observations agree well with the conclusion that surface charge-induced concentration polarization effects are an important force at play in delivery with nanopipettes.

#### Influence of delivery potential pulse width and amplitude on the delivered dosage

To further investigate the delivery capability of the carbon ring/nanopore electrode, bare nanopipettes filled with 100 mM KCl (pH = 8.0) and 2 mM  $FcTMA^+$  were examined with respect to two variables. The first variable studied was the pulse width of the delivery potential. Magnitudes of both the delivery potential and retaining potential were held constant.

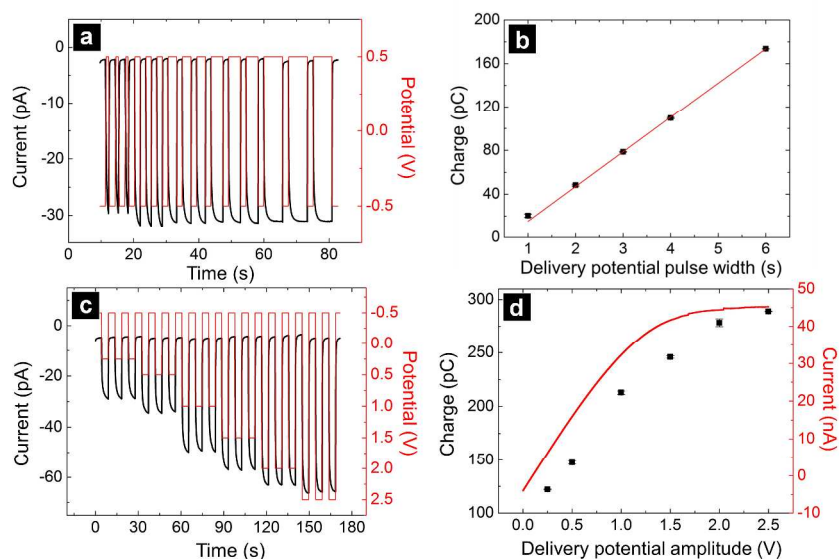


**Figure 4.** (a) Amperometric I-T curve collected by the carbon ring for FcTMA<sup>+</sup>, red trace: applied potential; black trace: current; the amplitude of the applied potential is kept at  $V_p = \pm 0.5$  V, the pulse width of the retaining potential is 1 s, and the pulse width of the delivery potential varies from 1 s, 2 s, 3 s, 4 s, 6 s, respectively. (b) Amount of charge delivered at different delivery potential pulse width; (c) I-T curve collected by the carbon ring for FcTMA<sup>+</sup>, red trace: applied potential; black trace: current. The frequency of the square wave is kept at 0.1 Hz, the retaining potential is kept constant,  $V_{\text{retaining}} = -0.5$  V, and the delivery potential amplitude is  $V_{\text{delivery}} = +0.25$  V,  $+0.5$  V,  $+1$  V,  $+1.5$  V,  $+2$  V and  $+2.5$  V, respectively. (d) Amount of charge delivered at different

Pulse widths of the delivery potential were held at 1 s, 2 s, 3 s, 4 s and 6 s. Detected current at the WE stayed nearly constant (**Figure 4a**). The amount of charge (denoted as  $Q$ , obtained by integration of the I-T response at each delivery potential interval) at various delivery potential's pulse width ( $T$ ), the Q-T curve is shown in **Figure 4b**. A linear relationship (red trend line) between the amount of charge delivered ( $Q$ ) and the delivery potential pulse width ( $T$ ) was obtained under these conditions. As the delivery potential was held at  $+0.5$  V, ion current in the delivery channel was constant, and thus dosage was determined solely by duration of the delivery potential, which led to a linear relationship between the amount of charge and the delivery potential pulse width. Consequently, even with ICR effects shown here, simply adjusting the pulse duration of the delivery potential, controls the amount of molecules delivered, in agreement with previous reports.<sup>3, 7, 45</sup> In addition, determination of the delivery amount is imperative. Herein, to quantify delivery, **equation 2** was used,

$$Q = znF \quad (2)$$

where  $Q$  is the amount of charge,  $z$  is the charge of the molecule of interest,  $n$  is moles detected, and  $F$  is the Faraday constant, the calculated amount of molecules detected is shown in **Table 1**.

To study the effect of delivery potential amplitude, the amplitude of the delivery potential was varied at  $+0.25$  V,  $+0.5$  V,  $+1$  V,  $+1.5$  V,  $+2$  V and  $+2.5$  V, while frequency of the square wave and magnitude of the retaining potential were kept

**Table 1.** Current amplitude, amount of charge detected, and amount of concentration measured at different delivery potentials and different delivery potential pulse widths.

Delivery potential (V)	$ i $ (pA)	$Q$ (pC) N=3	Concentration measured (pmole)
0.25	24.1	122.2 ± 0.5	1.26E-03
0.5	32.3	147.6 ± 1.5	1.53E-03
1	44.7	212.9 ± 1.6	2.20E-03
1.5	52.3	278.9 ± 3.5	2.88E-03
2	57.3	289.0 ± 0.3	2.99E-03
Delivery potential pulse width (s)	$ i $ (pA)	$Q$ (pC) N=3	Concentration measured (pmole)
1	26.9	20.5 ± 1.5	2.12E-04
2	29.2	48.4 ± 0.9	5.02E-04
3	28.5	78.5 ± 0.2	8.13E-04
4	28.3	109.5 ± 0.6	1.13E-03
6	28.5	174.5 ± 0.0	1.81E-03

constant, as illustrated in the I-T curve in **Figure 4c**. The amount of charge measured at the WE at each applied delivery potential, the Q-V curve, is shown in **Figure 4d**. The Q-V curve leveled off with increased delivery potential. The I-V curve collected from  $-2.5$  V to  $+2.5$  V with the same pipette used in the above experiment exhibited rectified current response (**Figure S3, Supporting Information**). When plotted on the same potential axis, the Q-V curve (as shown in black square symbols in **Figure 4d**) and the positive half of the I-V curve (as shown in red line in **Figure 4d**), display a similar trend under these conditions. At positive potentials, ion depletion occurs, therefore the diminished delivery for FcTMA<sup>+</sup> is attributed to the ion depletion at positive bias. In addition, the delivery of a neutral electroactive species vs. delivery potential amplitude was also examined. A bare carbon ring/nanopore electrode was filled with 2 mM FcMeOH together with 100 mM KCl (pH = 8.0), I-T curves were taken as the delivery potential amplitude was varied at  $+0.25$  V,  $+0.5$  V,  $+1$  V,  $+2$  V, while the frequency ( $f = 0.1$  Hz) and retaining potential magnitude ( $-0.5$  V) were kept constant (**Figure S4, Supporting Information**). A linear relationship (**Figure S5, Supporting Information**) was observed between the amount of charge delivered and the delivery potential amplitude for neutral FcMeOH, in agreement with previous reports.<sup>20, 26</sup>

To summarize I-T, Q-T and Q-V curves shown in **Figure 4**, the absolute value of the current magnitude ( $|i|$ ) and the amount of charge ( $Q$ ) detected WE are summarized in **Table 1**. As the delivery potential was kept constant at varying pulse widths,  $|i|$  stayed relatively constant ( $28.27 \pm 0.75$  pA), which agreed well with the qualitative analysis for **Figure 4a**. While as the delivery potential amplitude increased, both  $|i|$  and  $Q$  increased.

In **Table S1**, the difference of current magnitude at two adjacent delivery potentials ( $\Delta i$ ; e.g.  $|i_{1V}| - |i_{0.5V}|$ ) and the difference in the amount of charge delivered at two adjacent potentials ( $\Delta Q$ ; e.g.  $Q_{1V} - Q_{0.5V}$ ) are shown. Interestingly,  $\Delta I$

decreased from +1.0 V to +2.5 V. The same trend was observed for  $\Delta Q$ , a similar observation is shown in **Figure 4c, d**.

## Conclusions

We have demonstrated the effect of surface charge on delivery with nanopipettes. Results dependent on polarity of surface charge, electrolyte concentration, and potential of delivery were investigated. For bare quartz nanopipettes with negative surface charge, enhanced delivery for anions and diminished delivery for cations was obtained. For PEI-modified nanopipettes, concentration polarization effect is reversed and consequently, enhanced delivery for cations and diminished delivery for anions was obtained. These effects are expected to play a significant role, especially with small diameter pipettes, utilized in nanoscale deposition with tools such as scanning ion conductance microscopy. These effects are important at ionic strengths comparable to those (e.g. Ringer's Solution) utilized in cell/tissue studies, which further underscores the importance of these effects in nanopipette delivery in biological settings. As required in future studies, control of nanopipette surface charge – and in turn concentration polarization – may provide an additional handle to tune control of delivery.

## Acknowledgements

This work is financially supported by National Science Foundation CAREER Award (CHE 0847642). The Nanoscale Characterization Facility at Indiana University is acknowledged for FIB access that was acquired through the National Science Foundation MRI program (0923064).

## Notes and references

<sup>a</sup> Department of Chemistry, Indiana University, 800 E. Kirkwood Avenue, Bloomington, IN 47405 USA. E-mail: lanbaker@indiana.edu

<sup>†</sup> Electronic Supplementary Information (ESI) available: [supporting information as indicated in the text is available]. See DOI: 10.1039/b000000x/

1. C. A. Morris, A. K. Friedman and L. A. Baker, *Analyst*, 2010, **135**, 2190-2202.
2. C. Wei, A. J. Bard and S. W. Feldberg, *Anal. Chem.*, 1997, **69**, 4627-4633.
3. B. Babakinejad, P. Jönsson, A. López Córdoba, P. Actis, P. Novak, Y. Takahashi, A. Shevchuk, U. Anand, P. Anand, A. Drews, A. Ferrer-Montiel, D. Klenerman and Y. E. Korchev, *Anal. Chem.*, 2013, **85**, 9333-9342.
4. A. Bruckbauer, P. James, D. Zhou, J. W. Yoon, D. Excell, Y. Korchev, R. Jones and D. Klenerman, *Biophys. J.*, 2007, **93**, 3120-3131.
5. N. Calander, *Anal. Chem.*, 2009, **81**, 8347-8353.
6. N. Sa and L. A. Baker, *J. Electrochem. Soc.*, 2013, **160**, H376-H381.
7. L. Ying, A. Bruckbauer, A. M. Rothery, Y. E. Korchev and D. Klenerman, *Anal. Chem.*, 2002, **74**, 1380-1385.
8. L.-X. Zhang, X.-H. Cao, W.-P. Cai and Y.-Q. Li, *J. Fluoresce.*, 2011, **21**, 1865-1870.
9. A. Bruckbauer, L. Ying, A. M. Rothery, D. Zhou, A. I. Shevchuk, C. Abell, Y. E. Korchev and D. Klenerman, *J. Am. Chem. Soc.*, 2002, **124**, 8810-8811.
10. A. Bruckbauer, D. Zhou, L. Ying, Y. E. Korchev, C. Abell and D. Klenerman, *J. Am. Chem. Soc.*, 2003, **125**, 9834-9839.
11. R. Adam Seger, P. Actis, C. Penfold, M. Maalouf, B. Vilozny and N. Pourmand, *Nanoscale*, 2012, **4**, 5843-5846.

12. Y. Zhang and L.-C. Yu, *Curr. Opin. Biotech.*, 2008, **19**, 506-510.
13. A. Bruckbauer, P. James, D. Zhou, J. W. Yoon, D. Excell, Y. Korchev, R. Jones and D. Klenerman, *Biophys. J.*, 2007, **93**, 3120-3131.
14. R. W. Clarke, S. S. White, D. Zhou, L. Ying and D. Klenerman, *Angew. Chem. Int. Ed. Engl.*, 2005, **44**, 3813-3816.
15. K. T. Rodolfa, A. Bruckbauer, D. Zhou, Y. E. Korchev and D. Klenerman, *Angew. Chem. Int. Ed. Engl.*, 2005, **44**, 6854-6859.
16. L. Ying, A. Bruckbauer, D. Zhou, J. Gorelik, A. Shevchuk, M. Lab, Y. Korchev and D. Klenerman, *Phys. Chem. Chem. Phys.*, 2005, **7**, 2859-2866.
17. L. Ying, S. S. White, A. Bruckbauer, L. Meadows, Y. E. Korchev and D. Klenerman, *Biophys. J.*, 2004, **86**, 1018-1027.
18. F. O. Laforge, J. Carpino, S. A. Rotenberg and M. V. Mirkin, *Proc. Natl. Acad. Sci.*, 2007, **104**, 11895-11900.
19. J. D. Piper, C. Li, C.-J. Lo, R. Berry, Y. Korchev, L. Ying and D. Klenerman, *J. Am. Chem. Soc.*, 2008, **130**, 10386-10393.
20. M. Armstrong-James, K. Fox, Z. L. Kruk and J. Millar, *J. Neurosci. Meth.*, 1981, **4**, 385-406.
21. Z. L. Kruk, M. Armstrong-James and J. Millar, *Life Sci.*, 1980, **27**, 2093-2098.
22. M. Armstrong-James, J. Millar and Z. L. Kruk, *Nature*, 1980, **288**, 181-183.
23. N. R. Herr, A. M. Belle, K. B. Daniel, R. M. Carelli and R. M. Wightman, *ACS Chem. Neurosci.*, 2010, **1**, 627-638.
24. W. G. Kuhr and R. M. Wightman, *Brain Res.*, 1986, **381**, 168-171.
25. J. Cervera, B. Schiedt, R. Neumann, S. Mafé and P. Ramírez, *J. Chem. Phys.*, 2006, **124**, 104706.
26. M. L. Kovarik, K. Zhou and S. C. Jacobson, *J. Phys. Chem. B*, 2009, **113**, 15960-15966.
27. C. Kubeil and A. Bund, *J. Phys. Chem. C*, 2011, **115**, 7866-7873.
28. J. M. Perry, K. Zhou, Z. D. Harms and S. C. Jacobson, *ACS Nano*, 2010, **4**, 3897-3902.
29. Q. Pu, J. Yun, H. Temkin and S. Liu, *Nano Lett.*, 2004, **4**, 1099-1103.
30. R. B. Schoch, J. Han and P. Renaud, *Rev. Mod. Phys.*, 2008, **80**, 839-883.
31. Z. S. Siwy, *Adv. Funct. Mater.*, 2006, **16**, 735-746.
32. H. S. White and A. Bund, *Langmuir*, 2008, **24**, 2212-2218.
33. M. A. Derylo, K. C. Morton and L. A. Baker, *Langmuir*, 2011, **27**, 13925-13930.
34. K. C. Morton, M. A. Derylo and L. A. Baker, *J. Electrochem. Soc.*, 2012, **159**, H662-H667.
35. K. C. Morton, C. A. Morris, M. A. Derylo, R. Thakar and L. A. Baker, *Anal. Chem.*, 2011, **83**, 5447-5452.
36. R. Thakar, A. E. Weber, C. A. Morris and L. A. Baker, *Analyst*, 2013, **138**, 5973-5982.
37. S. Liu, Y. Dong, W. Zhao, X. Xie, T. Ji, X. Yin, Y. Liu, Z. Liang, D. Momotenko, D. Liang, H. H. Girault and Y. Shao, *Anal. Chem.*, 2012, **84**, 5565-5573.
38. A. Szabo, *J. Phys. Chem.*, 1987, **91**, 3108-3111.
39. J. L. Conyers and H. S. White, *Anal. Chem.*, 2000, **72**, 4441-4446.
40. D. Woermann, *Nucl. Instr. Meth. Phys. Res. B*, 2002, **194**, 458-462.
41. D. Hlushkou, J. M. Perry, S. C. Jacobson and U. Tallarek, *Anal. Chem.*, 2012, **84**, 267-274.
42. D. Woermann, *Phys. Chem. Chem. Phys.*, 2003, **5**, 1853-1858.
43. G. A. Parks, *Chem. Rev.*, 1965, **65**, 177-198.
44. S. J. Konopka and B. McDuffie, *Anal. Chem.*, 1970, **42**, 1741-1746.
45. Y. Takahashi, A. I. Shevchuk, P. Novak, Y. Zhang, N. Ebejer, J. V. Macpherson, P. R. Unwin, A. J. Pollard, D. Roy, C. A. Clifford, H. Shiku, T. Matsue, D. Klenerman and Y. E. Korchev, *Angew. Chem. Int. Ed. Engl.*, 2011, **50**, 9638-9642.

# TOC Figure

